nuclear fusion
IAEA

PAPER • OPEN ACCESS

Helium plasma operations on ASDEX Upgrade and JET in support of the non-nuclear phases of ITER

To cite this article: A. Hakola *et al* 2024 *Nucl. Fusion* **64** 096022

OPEN ACCESS
IOP Publishing | International Atomic Energy Agency
Nuclear Fusion
Nucl. Fusion **64** (2024) 096022 (15pp)
https://doi.org/10.1088/1741-4326/ad6335

Helium plasma operations on ASDEX Upgrade and JET in support of the non-nuclear phases of ITER

A. Hakola[1,*], M. Balden[2], M. Baruzzo[3], R. Bisson[4], S. Brezinsek[5], T. Dittmar[5], D. Douai[6], M. Dunne[2], L. Garzotti[7], M. Groth[8], R. Henriques[7], L. Horvath[7,13], I. Jepu[7], E. Joffrin[6], A. Kappatou[2], D. Keeling[7], K. Krieger[2], B. Labit[9], M. Lennholm[7], J. Likonen[1], A. Loarte[10], P. Lomas[7], C. Lowry[7], M. Maslov[7], D. Matveev[5], R.A. Pitts[10], U. Plank[2], M. Rasinski[5], D. Ryan[7], S. Saarelma[7], S. Silburn[7], E.R. Solano[11], W. Suttrop[2], T. Tala[1], E. Tsitrone[6], N. Vianello[12], T. Wauters[10], A. Widdowson[7], M. Wischmeier[2], the EUROfusion Tokamak Exploitation Team[a], the ASDEX Upgrade Team[b] and JET Contributors[c]

[1] VTT Technical Research Centre of Finland Ltd, Espoo, Finland
[2] Max-Planck-Institut für Plasmaphysik, Garching, Germany
[3] ENEA, Frascati, Italy
[4] CNRS, PIIM, Aix-Marseille University, Marseille, France
[5] Institut für Energie und Klimaforschung-Plasmasphysik, Forschungszentrum Jülich, Jülich, Germany
[6] CEA, IRFM, Saint-Paul-lez-Durance, France
[7] Culham Science Centre, UKAEA, Abingdon, United Kingdom of Great Britain and Northern Ireland
[8] Department of Applied Physics, Aalto University, Espoo, Finland
[9] Swiss Plasma Center, EPFL, Lausanne, Switzerland
[10] ITER Organization, St Paul Lez Durance Cedex, France
[11] Laboratorio Nacional de Fusión, CIEMAT, Madrid, Spain
[12] Consorzio RFX, ISTP, Padova, Italy
[13] Princeton Plasma Physics Laboratory, Princeton, NJ, United States of America

E-mail: antti.hakola@vtt.fi

Received 15 January 2024, revised 16 May 2024
Accepted for publication 15 July 2024
Published 31 July 2024

Abstract

For its initial operational phase, ITER has until recently considered using non-nuclear hydrogen (H) or helium (He) plasmas to keep nuclear activation at low levels. To this end, the Tokamak Exploitation Task Force of the EUROfusion Consortium carried out dedicated experimental campaigns in He on the ASDEX Upgrade (AUG) and JET tokamaks in 2022, with particular emphasis put on the ELMy H-mode operation and plasma-wall interaction processes as well as comparison to H or deuterium (D) plasmas. Both in pure He and mixed He + H plasmas, H-mode operation could be reached but more effort was needed to obtain a stable plasma scenario than in H or D. Even if the power threshold for the LH transition was lower in He, entering the type-I ELMy regime appeared to require equally much or even more heating power

[a] See Joffrin *et al* 2024 (https://doi.org/10.1088/1741-4326/ad2be4) for the EUROfusion Tokamak Exploitation Team.
[b] See Zohm *et al* 2024 (https://doi.org/10.1088/1741-4326/ad249d) for the ASDEX Upgrade Team.
[c] See Maggi *et al* 2024 (https://doi.org/10.1088/1741-4326/ad3e16) for JET Contributors.
[*] Author to whom any correspondence should be addressed.

than in H. Suppression of ELMs by resonant magnetic perturbations was studied on AUG but was only possible in plasmas with a He content below 19%; the reason for this unexpected behaviour remains still unclear and various theoretical approaches are being pursued to properly understand the physics behind ELM suppression. The erosion rates of tungsten (W) plasma-facing components were an order of magnitude larger than what has been reported in hydrogenic plasmas, which can be attributed to the prominent role of He^{2+} ions in the plasma. For the first time, the formation of nanoscale structures (W fuzz) was unambiguously demonstrated in H-mode He plasmas on AUG. However, no direct evidence of fuzz creation on JET was obtained despite the main conditions for its occurrence being met. The reason could be a delicate balance between W erosion by ELMs, competition between the growth and annealing of the fuzz, and coverage of the surface with co-deposits.

Keywords: helium plasma, H-mode, tungsten fuzz, erosion

(Some figures may appear in colour only in the online journal)

1. Introduction

Helium (He) will be formed in ITER and future fusion power plants as a result of deuterium–tritium (DT) fusion reactions ($^2H + {}^3H \rightarrow {}^4He + n$), expected to result in concentrations up to a few at.% in the plasma [1]. In addition, helium is, along with hydrogen (H), a potential plasma gas to be used in the initial, non-nuclear operational phases of a reactor to keep nuclear activation at low levels. The ITER Research Plan [2] has up to now put forward a strategy to use either H or He or, alternatively, both of them in a staged manner during this first operational step. ITER has therefore asked the EUROfusion Consortium to provide them with experiences on operations in pure He and mixed He + H plasmas. Recently, ITER has started a process to amend its Research Plan [3]. The present proposal includes abandoning the use of beryllium (Be) in the first wall and replacing it with tungsten (W), already selected as the plasma-facing material (PFM) at the divertor. In addition, the plan puts forward a streamlined approach to proceed towards DT plasmas as soon as possible, and this may lead to reducing the duration of the non-nuclear operations to their bare minimum. It is therefore even more important to fully assess and investigate all the aspects related to this paradigm change, including the implications to the initial low activation phase.

The task was adopted by the Tokamak Exploitation Task Force, under which dedicated experimental campaigns were designed and performed on the ASDEX Upgrade (AUG) [4] and JET [5] tokamaks in 2022, the latter equipped with the ITER-like Wall (ILW) since 2011. These devices have a high relevance for ITER: they have a W divertor and a metallic wall, consisting of W in AUG and Be in JET, they are equipped with versatile options for plasma heating using a combination of neutral beam injection (NBI) and ion cyclotron and electron cyclotron resonance heating (ICRH/ECRH), as well as exhibit broad diagnostics capabilities. There were also distinct differences between the two devices during the He operations (see section 2 for details), most notably that (i) the JET NBI system was converted into He while that of AUG was run in H/D and (ii) JET applied regularly the argon (Ar)-frosting technique to allow operations at low densities while no Ar frosting was used on AUG.

The main research objectives were (i) developing reliable H-mode scenarios in He with robust type-I Edge-Localized Modes (ELMs) [6], (ii) determining the power needed for the L- to H-mode transition and pedestal characteristics in the selected scenarios, (iii) studying power and particle transport in helium plasmas and He particle recycling, (iv) identifying possibilities for suppressing ELMs, (v) investigating various plasma-wall interaction (PWI) processes such as erosion of Be and W plasma-facing components (PFCs) and formation of nanoscale structures on W upon exposure to He discharges, and (vi) making a detailed comparison between the He experiments and the data collected from hydrogenic (H, D, T) plasmas.

Here we describe the experimental campaigns on the two devices (in section 2), give an overview of the main results obtained against the set objectives (section 3), and finally conclude and discuss the implications for ITER (section 4). We will show that there are several research areas that require further investigations, including detailed data analysis and interpretative modelling. This article will therefore act as a reference for the future publications where the underlying physics of the identified phenomena will be addressed in more detail.

2. Experiments on AUG and JET

2.1. AUG helium campaign

On AUG, a 2 week-long period in late July 2022 was dedicated to operations in helium plasmas. Both pure He and mixed He + D and He + H plasma discharges were executed by applying the ICRH, ECRH, and NBI heating schemes that had already been established in the previous He operational phases in 2015 and 2019 [7]. This time NBI was only operated in H and D, which somewhat limited the purity of the obtained plasmas, particularly in beam-heated scenarios. The density control was also hampered by the poor pumping characteristics of He. In 2015, an argon-frosting scheme was tested, in other words a layer of Ar frost was applied on the panels of the

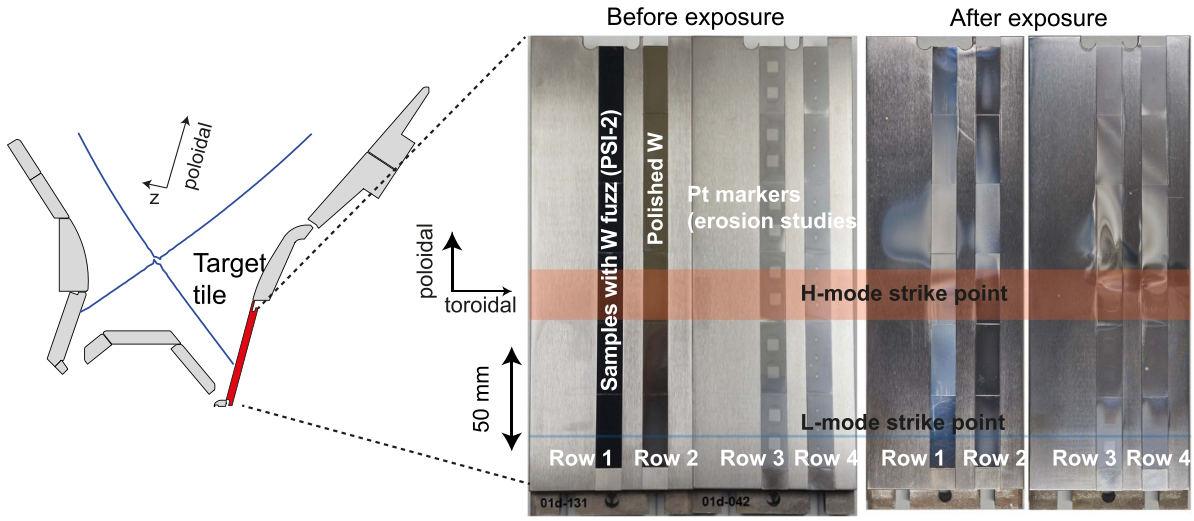

Figure 1. Poloidal cross section of the AUG divertor with the target tile for the DIM-II divertor manipulator marked in red (left) and photographs of the samples before and after their exposure on DIM-II (right). The poloidal locations of the L- and H-mode strike points are also marked in the figure.

divertor cryo pump. Contrary to the experience from JET [8], the improvement was marginal in reaching the lowest desired densities, in addition to which noticeable Ar pollution of the plasma was measured. For this reason, no Ar frostings were applied in 2022. The situation is expected to improve with the installation of a new charcoal-coated cryo pump in 2024 to enable efficient pumping of helium.

2.1.1. PWI studies at the divertor. During the AUG helium campaign, a special experiment was carried out where small marker samples were exposed to a sequence of L- and H-mode plasma discharges during a single session at the outer (low-field-side) strike-point (OSP) region using the DIM-II divertor manipulator of AUG [9]. The DIM-II target tiles were equipped with four poloidal rows of samples as follows, see figure 1:

- Bulk W samples with nanoscale surface features on them produced at the PSI-2 linear plasma facility [10] (Row 1)
- Polished bulk W samples (Row 2)
- W-coated (thickness ∼300 nm) graphite samples with small (5×5 mm^2 and 1×1 mm^2) platinum (Pt) marker spots (thickness ∼40–50 nm) on them (Rows 3 and 4)

The PSI-2 exposure aimed at producing nanoscale features and the so-called W fuzz (see [11, 12] for recent overviews) on the surface. Fuzz refers to hair-like nanotendrils that can grow on W surfaces following their exposure to a He particle flux with a high enough energy ($E_{\mathrm{in}} > 20$ eV) and a sufficiently large fluence ($>10^{24}$ m^{-2}) at surface temperatures exceeding 1000 K. Essentially, the process is initiated by the formation of nanoscale bubbles in the sub-surface layer where the bubbles will grow and coalesce and finally collapse leaving noticeable protrusions behind [12].

In the 2022 experiment, the idea was to see if one can initiate fuzz formation on originally virgin surfaces (polished W samples) in tokamak conditions and erode or modify the existing fuzz network (PSI-2 samples). In the H-mode discharges, the conditions were tailored to favour W fuzz growth while in the L-mode part, erosion was expected to dominate the PWI behaviour.

The samples with Pt markers, for their part, were designed to investigate erosion and deposition processes in helium plasmas and compare the data with existing results from similar exposures in deuterium [13]. Platinum was selected as the main marker material and a proxy for W due to the full-W coverage of the AUG vessel while graphite as the substrate made it possible to experimentally determine erosion of all the surface layers.

All the samples, their mounting on the DIM-II target tiles as well as the location of the OSP during the L- and H-mode phases of the experiment are illustrated in figure 1. The two strike points were separated by a distance of a few centimetres, thus resulting in distinct erosion peaks in each part of the experiment. The sequence was started with H-mode, after which the OSP was moved poloidally downwards to ensure that no extra coverage of the samples with deposits would occur except in a narrow region between the H- and L-mode strike lines.

2.2. JET C43 helium campaign

On JET, approximately two months of experimental time was dedicated to the helium plasma operations, referred to as the C43 campaign. The campaign was started with a detailed sequence of wall-conditioning pulses (6 sessions) and then continuing the activities in helium plasmas, ultimately reaching purity levels of >99% during C43. A few individual sessions were devoted to mixed He + H plasmas, mainly for

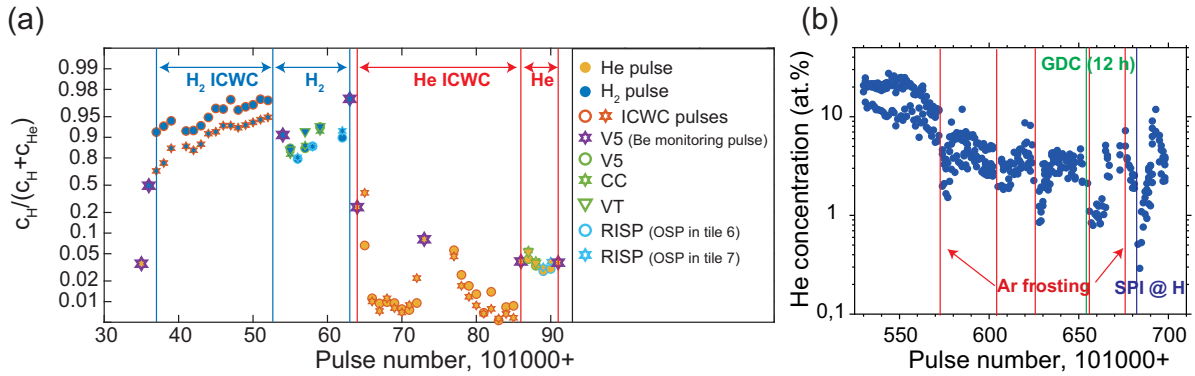

Figure 2. (*a*) Measured H/(H + He) concentration during the He → H and H → He changeover experiments at JET, based on OGA data. Here, V5, CC, VT, and RISP stand for different plasma configurations as described in [16]. (*b*) Evolution of the He concentration in the JET plasma after the C43 He campaign. The Ar frostings, GDC cleanings, and SPI operations are marked with red, green, and blue vertical lines, respectively.

LH-transition investigations. A large fraction of the campaign time was spent on developing ELMy H-mode scenarios and PWI investigations, using here mainly NBI for plasma heating and H-minority ICRH in selected experiments. The JET NBI system was converted from D to He, which unfortunately limited the available beam power to ∼13 MW and thus setting a strong restriction on the H-mode operational space during the campaign.

Regular argon frostings were applied on the JET cryopanels throughout the C43 campaign, successfully enhancing the He pumping capabilities of the vessel [8]. Around 50 bar l of argon applied during the frosting stages in the beginning of and during the experimental days was noticed to be sufficient for maximum pumping of helium such that the desired low density levels in the plasma could be reached. Topping up the frosting by 20 bar l of Ar after each discharge could maintain the efficient pumping throughout a series of pulses. It is worth noting that Ar frosting is a method required in present-day devices to improve helium pumping while ITER does not require this approach since it will use special activated charcoal cryopumps that can efficiently control the helium content in the vessel [14].

2.2.1. Wall conditioning investigations. Wall conditioning was performed during the first three days of C43 by carrying out back-and-forth transitions from helium to hydrogen and hydrogen to helium (He → H and H → He, respectively) [15]. During these changeover phases, approximately 16 s long ion cyclotron wall conditioning (ICWC) pulses [16, 17] were carried out with the coupled RF power being in the range of 0.16 MW for H-ICWC (He → H) and 0.24 MW for He-ICWC (H → He) [17]. After each step, a series of pre-designed, ICRH-heated plasma pulses in the limiter and divertor configurations (either in H or He) was carried out to study the evolution of the plasma purity. The selected divertor configurations were the JET standard V5 (inner strike point on the vertical target, tile 3, and OSP on tile 5), VT (both strike points on the vertical targets, tiles 3 and 7), CC (strike points at the divertor lower corners), and RISP (Raised Inner Strike Point) where the inner strike point (ISP) was located as much up on tile 1 as possible and the OSP either on tile 6 or tile 7. Details and illustration of the applied configurations can be found in [16]. In all cases the power level was kept <2 MW.

The overall changeover sequence consisted of 15 ICWC discharges in H, 6 plasma pulses in H, 17 ICWC discharges in He, and finally 4 plasma pulses in He, see figure 2. Argon frosting with cold cryopanels was applied from the middle of the He-ICWC session onwards to enhance the pumping capabilities and speed up the conditioning. The results proved that the selected approach of combining ICWC with standard plasma discharges was an efficient way to re-condition the vessel walls and remove previous gas remnants. Starting from ∼3.6% of H in He, the peak hydrogen concentration reached in the H-plasma phase was >97% while in the back transition, one could finally return to H levels of ∼3.7% in He plasmas. The data were obtained by combining the results from optical emission spectroscopy in the plasma, optical gas analysis in the subdivertor region (OGA, Penning gauges), and residual gas analysis (RGA) further down in the pumping system [15].

Generally, the back transition H → He was faster than the forward one (He → H) as figure 2(*a*) shows. This was evidenced by the measured levels of residual gas (either He or H) in the regular plasmas following the ICWC steps. The residual He content in H plasmas varied between 3 and 20%, being the largest when applying diverted plasma pulses (15% on average) while the H content in He plasmas almost instantaneously dropped to <4%, both in the case of limiter and divertor discharges.

The qualitative difference between H and He became even clearer after the JET He campaign when a persistent He contamination of 3%–4% was observed during more than a week of D plasma operations, despite regular Ar frostings and long (∼12 h) glow discharge cleanings (GDC) in D. This behaviour is summarized in figure 2(*b*). In the end, disruptions with shattered hydrogen pellets (SPI in H) were effective in decreasing the He content to <1%. All this shows that special effort needs to be put on helium pumping and re-conditioning

of the wall following a He campaign. The results are in a good agreement with what was observed on WEST during its C4 campaign, following a sequence of changeovers D → He, He → D, and again D → He [15].

The RGA measurements provided additional insights into the different behaviour of H and He during the changeover experiment. The helium pulses exhibited a higher retention of He than removal of H but, on the other hand, the amount of He retained during the H → He phase was comparable to what could be removed in the He → H step by the H pulses. The H plasmas, for their part, were equally efficient in removing He than leaving H retained on the walls, and as a result, the overall H retention was ∼5 times larger than H removal during the entire experiment and a factor of 4 larger than the corresponding numbers for He [15]. The results imply that even though the retention of H may be high on the PFCs, its impact on the impurity content of the plasma is negligible due to the good pumping efficiencies of hydrogenic isotopes. On the other hand, the situation was changed during long-term outgassing after the changeover where the peak in the H outgassing rates was much delayed from the value reached at the end of the experiment similarly to what was observed in the C4 campaign of WEST [18]. This indicates that in ITER, the different release and retention dynamics have to be taken into account when designing plasma operations in H or He.

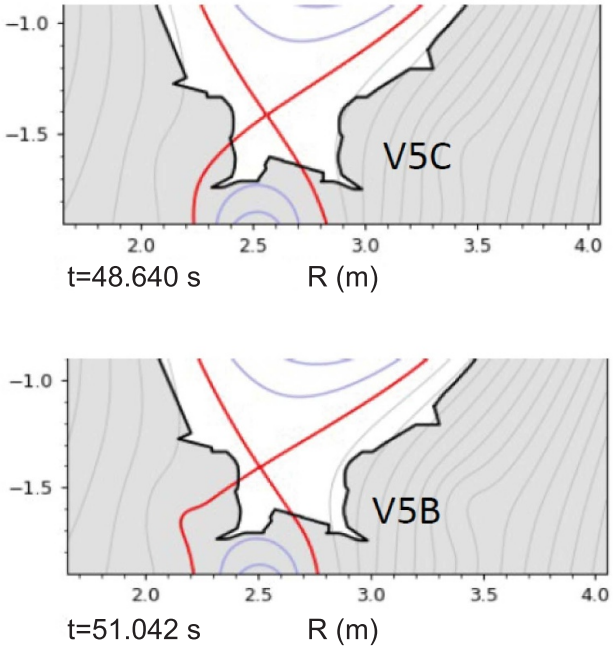

Figure 3. Difference between the standard V5C (top) and the newly developed V5B (bottom) configurations in the poloidal cross section of the JET divertor. The W fuzz discharges were started from V5C and then moved to V5B for the actual exposure.

2.2.2. High-fluence exposure of bulk W tiles. One week of the JET C43 campaign was devoted to an experiment to study possible formation of W fuzz as well to obtain information on erosion characteristics of W at the OSP region of the torus. Altogether 54 discharges were executed to accumulate enough fluence on the PFCs, especially on tile 5. To this end, a new scenario was developed with the outer strike point located on the so-called stack B of the tile, a region that is seldomly used in any plasma experiment and that was decided to be kept protected from any further plasma exposure in the subsequent operational phases of JET. The magnetic equilibrium of this V5B configuration is shown in figure 3, together with the standard V5C configuration.

3. Overview of experimental results

3.1. ELMy H-mode operation in He

ELMy H-mode operation, especially the transitions from L-mode into H-mode (LH transition) and further into the type-I regime (type III → I transition) as well as the resulting characteristics of the H-mode pedestal, were studied both on AUG and JET helium plasmas. On AUG, scenario development had been performed during the previous helium campaigns in 2015 and 2019 and they provided a good starting point for further investigations both with low and high triangularities (δ). The applied heating methods were NBI, ECRH, and NBI + ECRH to enable comparison between different approaches and with the existing H/D database [19], though recalling from section 2.1 that no He-NBI was carried out on AUG.

On JET, earlier experiments in 2019–2021 had documented the LH transition power threshold, P_{LH}, in He plasmas using either H-minority ICRH (with 2%–3% of hydrogen) or D-NBI [20] in the V5 configuration (plasma current $I_{\mathrm{p}} = 2.0$ MA, toroidal field $B_{\mathrm{t}} = 2.4$ T) and the CC configuration ($I_{\mathrm{p}} = 1.7$ MA, $B_{\mathrm{t}} = 1.8$ T). In all cases the helium fraction ($n_{\mathrm{He}}/(n_{\mathrm{He}} + n_{\mathrm{H}} + n_{\mathrm{D}})$ was greater than 90% at the time of the transition. It was shown for each dataset that the density at which the power threshold is minimum, $n_{\mathrm{e,min}}$, is considerably higher in He than in hydrogen and the lowest in deuterium plasmas, and that both, $n_{\mathrm{e,min}}$ and P_{LH} depend on the plasma configuration as well as the plasma species, $n_{\mathrm{e,min}}$ being lower for CC. Although P_{LH} is lower in the V5 configuration (about half at given density in the high-density branch), operation in CC is known to allow easier access to lower densities and to type-I ELMs. ELMs were observed in He plasmas at JET in the V5 configuration using the 1.2 MA/1.8 T scenario [21, 22], but most likely in type III.

The limited He-NBI power available in 2022 significantly restricted the parameter space of the possible He scenarios with steady type-I ELMs. In the end, the most robust type-I ELMy phases were obtained using the 1.3 MA/1.3 T scenario in the CC configuration [23]. This allowed comparison between H, D, and He plasmas. Another case studied was the one with 1.7 MA/1.8 T, which was also the choice in the carbon-dominated era of JET (JET-C) [24, 25]. Unfortunately, in the C43 campaign, no steady type-I ELMy phases were

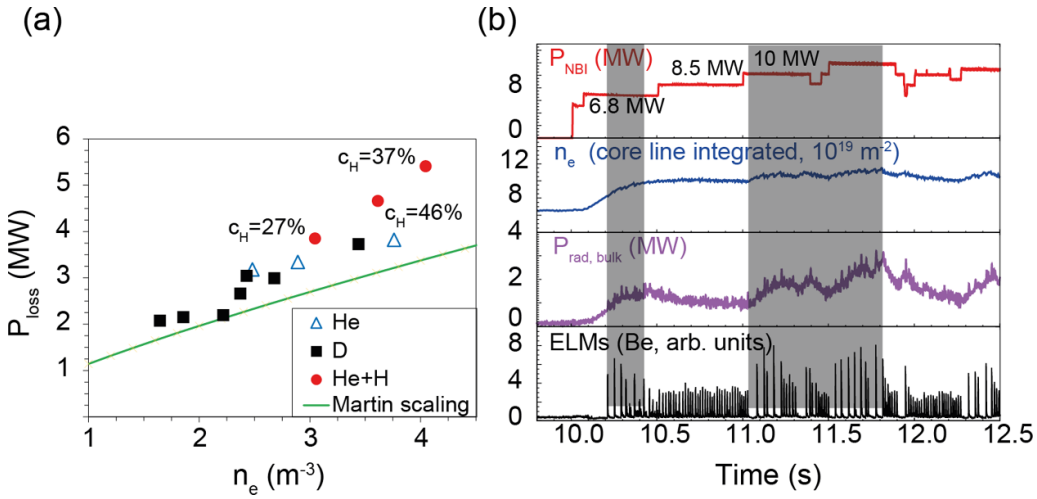

Figure 4. (*a*) Threshold power for the LH transition (in terms of the P_{loss} [21]) as a function of line-averaged density in selected CC plasmas at JET together with the Martin scaling. The H concentrations of the mixed H + He plasmas are marked in the plot next to the corresponding red circles. (*b*) Examples of time traces for the heating power, line-integrated density, bulk radiation, and ELM activity (in terms of Be emission) for the JET pulse 101 445 (1.3 MA/1.3 T). Type-I ELM activity is denoted by gray rectangles, with stable III→I transition obtained above 10 MW (>11 s).

observed in the 1.7 MA/1.8 T scenario with the available heating power, though LH transitions were documented.

3.1.1. LH transition in helium. Both on AUG and JET, H-mode operation could be achieved in helium but entering the type-I ELMy regime turned out to be more challenging than in H or D. Figure 4(*a*) shows P_{LH} as a function of the plasma density for selected JET CC discharges, both in pure and mixed He + H plasmas [20]; in the LH transition experiments on AUG, $n_{e,min}$ does not change with the plasma composition [19]. In pure He, and above $n_{e,min}$(He), P_{LH} is comparable to the values measured in D, i.e. $P_{LH}(D) \approx P_{LH}(He)$ while at similar densities in H higher heating powers are required such that $P_{LH}(H) \approx 2 \times P_{LH}(He)$ [19–21]. Figure 4(*a*) also shows the Martin scaling, the dependence of P_{LH} on various physical and engineering parameters such as plasma density (n_e), toroidal magnetic field (B_t), and plasma surface area (S). In D plasmas, the Martin scaling takes the form $P_{LH,Martin} \propto {n_e}^{0.717} {B_t}^{0.803} S^{.941}$ [26]. According to [19], the LH transition is strongly influenced by the local radial electric field interacting with edge turbulence, indicating that obtaining a proper understanding of the differences between P_{LH} in H, D, and He requires careful investigation of these aspects.

Considering mixed He + H plasmas, on AUG the focus was on H plasmas, whose He content was gradually increased. The helium-like characteristics started to appear once the He concentration (n_{He}/n_e) exceeded the level of c_{He} = 25%–30%: above this limit one can effectively consider the situation a He plasma seeded with hydrogen impurities [19]. In the opposite case of adding H into He plasmas, experiments were performed at JET (see figure 4(*a*)). Here, the dilution of the plasma led to an apparent increase (by 25%) of the LH threshold at H concentrations of (n_H/n_e) of c_H = 45% [20]. In any case, mixed discharges appear to behave differently from a pure H or He plasma. When considering the options for running non-nuclear operations in ITER, it remains uncertain if using helium would allow larger margins for reaching ELMy H-mode than hydrogen.

Above the LH transition, typically small and frequent type-III ELMs are first observed while entering the type-I ELMy region with elevated confinement requires even higher heating powers. An example of this III→I transition in one of the investigated JET discharges is visible in figure 4(*b*) around 10 MW of the applied heating power. While in D the limit is $P_{III→I}(D) = 1.0–1.5 \times P_{LH,Martin}$, in He plasmas much more heating is required to trigger type-I ELMs, of the order of $P_{III→I}(He) = 2.5–3.0 \times P_{LH,Martin}$. Our results also show that in H, the threshold $P_{III→I}(H)$ can be comparable to or not clearly larger than the corresponding value in He, $P_{III→I}(He)$. This is evidenced by the fact that $P_{III→I}$ in mixed He/H plasmas is at least not higher than in pure He while it can even be lower in certain plasma conditions. As a conclusion, even if or when P_{LH} is higher in H than in He, entering the type-I ELMy regime may require comparable amounts or even less heating power in H than in He [20].

Figure 4(*b*) also shows that, besides the high $P_{III→I}$, bulk radiation remains at a considerable level in He plasmas at least on JET. This can be partly attributed to efficient sputtering of W by He and Be impurities (see section 3.4.1) and results in ELMs easily becoming unstable. In figure 4(*b*) the trend is visible around 11.25 and 11.40 s, corresponding to peaks in the measured core radiation. It is thus possible that the primary reason for the increased III → I transition in He is closely linked to the elevated levels of radiated power. In comparable D discharges with lower levels of radiation, access to type-I ELMs happens straight away after the LH transition [20] but a detailed analysis is still pending to properly understand the different physics between H/D and He plasmas.

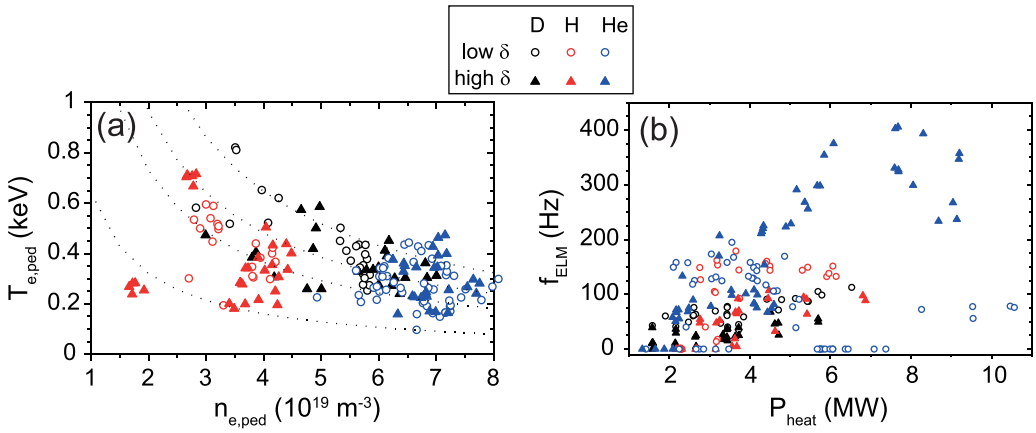

Figure 5. (*a*) Pedestal temperature as a function of the pedestal density for comparable AUG discharges in H (red), D (black), and He (blue) at low and high values of the triangularity δ. The dotted lines show a few examples of a constant pedestal pressure p_{ped}. (*b*) ELM frequency as a function of heating power for the same discharges.

Comparison to He experiments performed in JET-C show yet another striking difference in the LH and III $\rightarrow$ I transition characteristics. In the JET-C experiments, robust type-I ELMs could be achieved in He and at much more modest power levels than in the ILW phase: the data suggest that $P_{\mathrm{III}\rightarrow\mathrm{I}}$(He,JET-C) $\approx 1.6 \times P_{\mathrm{LH,Martin}}$ [24, 25]. We can therefore conclude that the wall material has a drastic impact on the operational space in helium. A caveat in the interpretation, though, is that the JET-C data has been extracted from studies in the 1.7 MA/1.8 T configuration while in JET-ILW, as stated above, the absence of steady type-I ELMs forced to base the discussion on the 1.3 MA/1.3 T scenario. On the other hand, in both scenarios the big type-I ELMs were relatively similar and occurred at the same low frequency of 20–30 Hz [20, 25]. In JET-C the divertor geometry was also different from that used in JET-ILW, meaning that the edge and transport properties of the plasmas were not identical.

3.1.2. Pedestal properties in H-mode in helium. The pedestal properties of different L- and H-mode helium plasmas were compared to the existing data sets collected from hydrogenic plasmas as well as to the available JET-C results [25]. The AUG pedestal database is much more extensive and the main results of the analyses are illustrated in figure 5. One notices that the pedestal heights in He are generally similar to those extracted in D or H, both for the electron density (n_{e}) and temperature (T_{e}) in otherwise comparable scenarios. The data originates from an established scenario for all the three gases with $I_{\mathrm{p}} = 0.8$ MA and $B_{\mathrm{t}} = 2.5$ T at different values of the plasma triangularity δ. For He, some 2–3 times higher heating powers were required to reach the same pedestal pressure (p_{ped}, dashed lines in figure 5(*a*) for a few examples) as in D. Another difference between He and H/D can be noticed from the measured ELM frequencies in figure 5(*b*). In helium, frequent ELMs are always measured especially towards higher heating powers and at high triangularities; at lower values of P_{heat} and at low triangularities, the data sets for H and He are comparable and ELM frequencies range from 100 to 200 Hz. In addition, they cannot be clearly categorized as type-I ELMs anymore but show features characteristic of type-III ELMs. Even a rollover effect is visible at the highest heating levels (above 8 MW in figure 5(*b*)).

On JET, the starting point was the 1.7 MA/1.8 T scenario (see section 3.1.1). Comparison to JET-C results revealed that, besides the III$\rightarrow$I transition, the wall material has a drastic impact on pedestal properties as well: even if the pedestal densities could be made equal, in JET-C the pedestal temperature was almost a factor of 2 higher and the discharges generally close to the peeling-ballooning boundary unlike in JET-ILW [25]. In another series of experiments with 1.0 MA/1.0 T, correlations between pedestal heights in D and He were assessed. Type-III ELMs were reached but volumetric radiation losses tended to increase rapidly above the LH transition thus making ELMs quickly irregular, analogously to what was discussed in section 3.1.1. Similarly to AUG, the pedestal height for T_{e} did not show noticeable differences between D and He but the limited heating power during C43 prevented from reaching a solid conclusion. Preliminary modelling with Europed/EPED [27] correctly reproduces the pedestal height in the 1.0 MA/1.0 T case while a massive overprediction results for the 1.7 MA/1.8 T plasmas, presumably because of deviations from the peeling-ballooning limit. Further work is therefore required for JET pedestal analysis.

3.2. Suppression of ELMs using resonant magnetic perturbations in helium

In addition to type-I ELMy H-mode operation, the complete suppression of ELMs by resonant magnetic perturbations (RMPs) was studied on AUG. The starting point was a well-characterized scenario with $I_{\mathrm{p}} = 0.9$ MA and $B_{\mathrm{t}} = 1.8$ T, where ELM suppression could be routinely obtained in D plasmas, provided that the safety factor, q_{95}, and the pedestal density, $n_{\mathrm{e,ped}}$, are kept within their experimentally determined boundaries: $q_{95} = 3.57$–3.95 and $n_{\mathrm{e,ped}} < 3.3 \times 10^{19}$ m^{-3} [28]. In

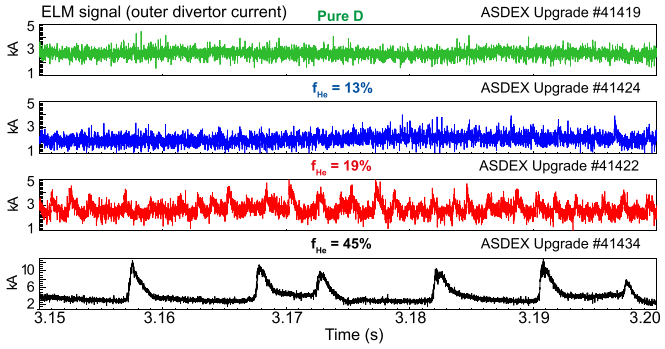

Figure 6. Time traces for the ELM footprints of selected AUG discharges with varying concentrations (f_{He}) of He in the plasma. Adapted from data in [29].

the series of discharges reviewed here, the He concentration ($n_{\mathrm{He}}/n_{\mathrm{e,ped}}$) was gradually increased from 0 to 45%, starting from a pure D plasma during the plasma changeover D $\rightarrow$ He. The heating powers were $P_{\mathrm{NBI}} = 5.9$ MW and $P_{\mathrm{ECRH}} = 2.3$ MW, and RMPs with a toroidal mode number of $n = 2$ were applied. The q_{95} and $n_{\mathrm{e,ped}}$ conditions were fulfilled except for the case with He concentration of 45% where the pedestal density could not reach low enough values due to limited He pumping capabilities.

The surprising outcome was that with the increasing He fraction, the discharge characteristics changed from complete ELM suppression (0%) to ELMs becoming intermittent (around 13%) and finally to their full re-appearance (>19%) [29]. Examples of the time traces for the ELM activity with different helium concentrations are illustrated in figure 6, showing especially the pattern of large ELMs at the highest helium levels. The reason for the characteristic difference between He and D plasmas is not understood yet and no obvious explanation is provided by the measured radial plasma profiles, especially for the electron density, electron and ion temperatures, and plasma rotation [29]. For the 13% and 19% He concentrations, these radial profiles are practically identical albeit between these values a qualitative change in the ELM behaviour takes place according to figure 6.

It is worth pointing out that also in hydrogen or mixed H + D plasmas the ELM suppression is lost on AUG once the H concentration is too high: earlier experiments have identified a limit of 40% after which small mitigated ELMs start to emerge [30, 31]. All this suggests that an established theory for ELM suppression by RMPs is needed to explain the peculiar empirical observations. Work is ongoing to test various ideas and even the validity of the ideal peeling-ballooning theory in He plasmas [29–31].

3.3. Transport and recycling characteristics in helium

Power and particle transport in helium plasmas as well as recycling of helium particles in the edge plasma were studied both on AUG and JET, mainly during L-mode discharges. On AUG, validating the existing transport models in different

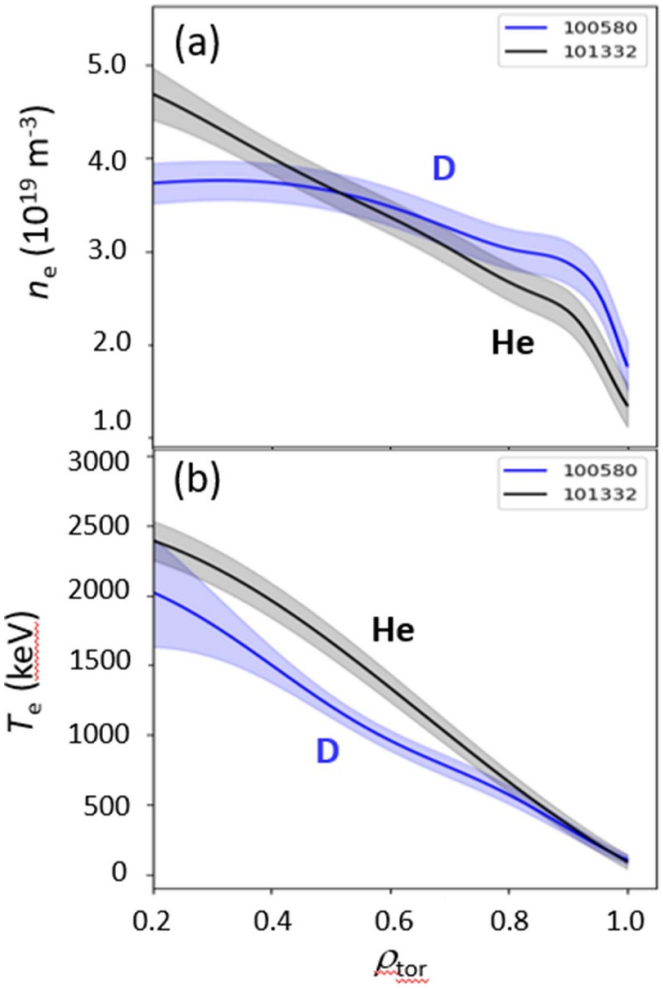

Figure 7. Profiles of (*a*) electron density and (*b*) electron temperature as a function of the normalized toroidal flux coordinate for dimensionally matched D (blue) and He (black) discharges on JET.

plasma gases could also be carried out during LH-transition experiments (see section 3.1.1).

3.3.1. Power and particle transport in L-mode. On AUG, effort was put on comparing the transport in H, D, and He plasmas in a scenario where a good database already exists from H and D, i.e. $I_p = 1.2$ MA, $B_t = 2.5$ T, and $q_{95} = 3.5$ [32, 33]. In terms of the plasma confinement, no noticeable differences could be recorded between the three gases; only the density is typically higher in helium. This suggests similar heat-transport characteristics in hydrogenic and helium plasmas. Understanding the differences or similarities in particle transport would require more detailed analysis of the executed discharges and modelling efforts, e.g. using a combination of ASTRA-TGLF and QuaLiKiz modelling [32, 33]. These would also cast light on the apparent discrepancies between the present and the published results: in [34], analysis and modelling efforts indicated a reduced confinement at the edge of He plasmas on AUG.

On JET, on the other hand, the focus was put on obtaining dimensional and dimensionless matches between D, T, and He plasmas, analogously to the analysis in [35], and this way provide more insights on the physics behind heat and particle transport. An example of the plasma profiles for dimensionally matched D and He discharges (in L-mode) can be found in figure 7, in both cases the applied heating power was $P_{\mathrm{NBI}} = 1.7$ MW. The electron temperature appears to be higher in helium but because the ion density (n_{i}) is a factor of two smaller in He than in D due to the difference in their charge numbers, the thermal energy W_{th} will become comparable in the two cases—similarly to what has been observed on AUG. This provides additional confirmation that the confinement and thus heat transport are not dramatically changed upon transition from D to He. On the other hand, electron density profiles in He plasmas were in the studied discharges more peaked than in D, suggesting clear changes in the particle transport picture. The dimensionless comparison between D and He discharges ($P_{\mathrm{NBI}} = 2.0$ MW in D, $P_{\mathrm{NBI}} = 4.4$ MW in He) also reveals peaked density profiles, thus the results in figure 7 are not a coincidence. One should note that earlier studies in JET-C suggested confinement in He plasmas to be some 60% of that in the reference D discharges but besides the different wall material, all the studies had been carried out in H-mode while now the work was exclusively in L-mode [25].

3.3.2. Recycling and detachment in L-mode. For the recycling studies, either fuelling or seeding (with nitrogen (N)) ramps were applied at varying heating powers. On AUG, up to 9 MW of ECRH and NBI were used while on JET, the data comes from fuelling-ramp experiments at fixed NBI powers around 5.0 MW. On both devices, the radiation patterns as well as the ion saturation currents were recorded as a function of the plasma density. Emphasis was put on determining the onset of detachment in the different cases.

With increasing density, peak radiation started to move from the inner towards the outer divertor and finally to the X-point region. This behaviour is analogous to the observations made in D, suggesting that the main radiator in the helium plasmas would indeed be the helium particles. Analysis of the relevant AUG and JET discharges further reveals that the total radiated power above the rollover density, the point where transformation from a high-recycling to a detached state of the divertor plasma begins, is >35% higher in He than in D. In addition, the measured neutral pressures in the subdivertor region are clearly lower and, most importantly, some 20% larger edge densities are required to exceed the rollover point in He than in D. The latter observation was accompanied by broader and shallower profiles for the ion saturation current at the divertor targets compared to what is typically the case in D. Examples of the measured ion saturation current profiles are illustrated in figure 8.

The observations imply significantly reduced recycling of neutrals in He compared to otherwise identical D plasmas [36]. This is not a completely unexpected result since the effective

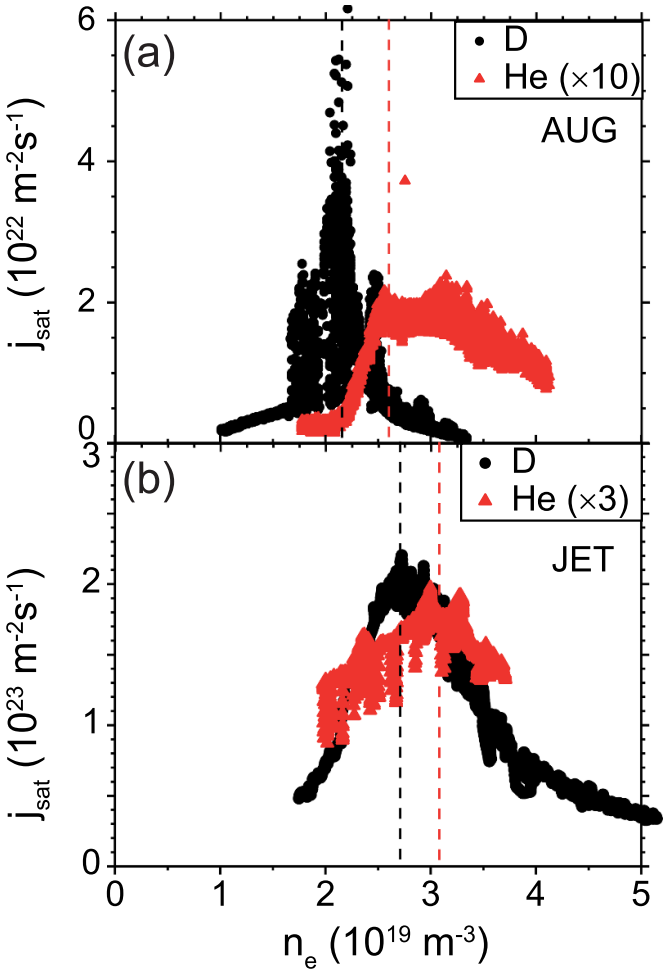

Figure 8. Ion saturation current as a function of the electron density of the plasma for comparable D (black) and He (red) discharges on (*a*) AUG and (*b*) JET.

ionization mean-free path of a neutral He atom would be some 2–3 times longer than that of a D neutral. On the other hand, charge-exchange-reaction chains are almost completely absent in He while they are very prominent in D, which essentially leads to generation of more D neutrals which are migrating in a random-walk manner and effectively would penetrate deeper into the plasma than is the case for He. However, especially the dramatic qualitative changes in the detachment characteristics require additional ingredients to fully understand the underlying physics. A plausible explanation to the observations could be the absence of molecules in He plasmas, thus the lack of channels where molecular dissociation would assist detachment via increased momentum and power losses [37]. As a result, the onset of detachment would require even higher densities in He, up to the values where electron-ion recombination finally takes over. Simulation efforts to verify or disprove this hypothesis are ongoing.

As in H or D, nitrogen seeding helps reaching the low electron temperatures of <2 eV, indicating no fundamental physics differences from the established picture of detachment in the different plasma gases.

3.4. PWI investigations in helium

PWIs in helium differ in three different ways from the established erosion-deposition picture in hydrogenic plasmas [7, 22]. First, the larger mass ($A = 4$) and charge ($Z = 2$) of helium compared to H or D will result in enhanced sputtering of PFCs, particularly due to the contribution of He^{2+} ions. The second main difference is the chemical passivity of helium, meaning that no chemically assisted erosion processes, e.g. the observed CAPS (Chemically Assisted Physical Sputtering) phenomenon of Be PFCs on JET via the formation of Be-D or Be-H molecules [38, 39] is expected to take place. Finally, the possible formation of nanoscale features, including fuzz, on W PFCs will change their erosion characteristics, thermo-mechanical properties, as well as retention of H isotopes in later operational phases [13, 40, 41]. In the following, we will address all these three key features in detail. For the discussion, it is worth distinguishing between gross and net erosion: gross erosion refers to how material is primarily released into the edge plasma via sputtering while net erosion takes into account re-deposition promptly and following migration in the scrape-off layer (SOL) plasma. Depending on the plasma conditions and the investigated PFC material, net erosion can be only a small fraction of gross erosion. Typically, gross erosion is determined spectroscopically while proper assessment of net erosion requires careful *post mortem* analyses of PFCs after relevant plasma operations.

3.4.1. Erosion of W and Be in helium. Information on W erosion was obtained both from the divertor-manipulator experiment on AUG (see section 2.1.1) as well as from a series of helium discharges carried out on JET during the above-mentioned 2019 experiment [22]. In the C43 campaign, the limited NBI power and additional issues with the machine and its subsystems did not allow to deepen the analyses to a wider range of scenarios, thus in the following we will briefly review what is known of W sputtering in L- and H-mode helium plasma discharges and complement the data of new findings available from AUG.

The JET data [22] indicate that W erosion at the divertor is dominated by intra-ELM sputtering: the erosion rates during ELMs can be a factor of 4 larger than in the inter-ELM phase. This conclusion remains valid both in He and in H/D, however, the helium data has been collected only from scenarios with relatively frequent ELMs (90–120 Hz) while in the D data set the range of ELM frequencies is 30–80 Hz. Despite these caveats, one can state that the sputtering rates per ELM are 1.5–3 times higher in He and do not decay as rapidly with increasing ELM frequency as in D plasmas. In addition, the difference in the sputtering rates between the inner and outer divertor targets is more noticeable in helium: some 2–3 times higher sputtering rates are measured at the outer side and this in/out asymmetry does not strongly depend on the ELM frequency. In the inter-ELM phase, for its part, an additional contribution comes from the presence of impurities in the plasma; in the JET case this means predominantly Be. At high divertor temperatures ($T_e > 20$ eV) the main sputtering agent is He^{2+} while below this limit, Be^{2+} is exclusively responsible for W sputtering.

The net erosion data of W has recently become available from the analysis of the exposed Pt marker samples from AUG [42]. The immediate first observation is that net erosion is largely amplified in He compared to the situation in D, by a much larger ratio than is the case for gross erosion. Close to the H-mode strike point, even complete disappearance of the marker coatings is measured, i.e. the corresponding net-erosion rate would be several nm s^{-1}. This is to be compared with the approximate value of <1.0 nm s^{-1} for D in H-mode [13]. In L-mode discharges with characteristics comparable to the inter-ELM part of the H-mode scenario, the erosion rates drop to much more modest values of the order of 0.1–0.2 nm s^{-1} which are in line with what the published data for D in [13] indicate. Note, however, that the D data is extracted from the erosion of gold and molybdenum (Mo) markers which may show somewhat different erosion characteristics than platinum, let alone tungsten. An interesting additional observation is that the eroded area on the L-mode strike point is very narrow whereas around the H-mode strike line the measured erosion is more profound and the extent of the affected zone extends poloidally deep into the SOL, in accordance with what was reported in [13] for a limited set of samples during the 2019 helium campaign on AUG. Inhomogeneous Pt layer erosion was observed throughout the samples and it could be attributed to the micrometer-scale surface roughness of the marker samples. Deposition was prominent below the L-mode strike point and in between the H- and L-mode strike lines, in the respective private flux regions, and mainly contained W (from surrounding regions on the divertor) and C (from erosion of the graphite substrates of the marker samples). A more in-depth discussion on the results can be found in [42].

In the case of Be, the focus was on studying the impact of CAPS on the erosion characteristics of Be PFCs. In H or D plasmas [38], CAPS results in the Be erosion yield showing a clear dependence on the wall temperature (T_{surf}) such that erosion is the highest at low values of T_{surf} while the temperature dependence practically vanishes above 350 °C, In contrast, no such trend was expected to appear in He. In the JET helium experiment, a series of L-mode limiter pulses ($I_p = 2.0$ MA, $B_t = 2.4$ T) was carried out by heating the limiter gradually at a rapid pulse repetition rate to >350 °C and after each pulse spectroscopically determining the erosion rate. Very surprisingly, a CAPS-like behaviour could be noticed as figure 9 illustrates for the measured Be II signal as a function of the JET pulse number (and thus with T_{surf}). The possible reasons for this puzzling observation will be discussed elsewhere but the most plausible explanation could be related to residual H or D atoms in the co-deposited layers on the JET PFCs: chemical reactions between the released hydrogenic atoms and Be could boost up the apparent Be erosion as visible in figure 9. Of course, one cannot fully exclude the possibility that the D (and H) inventories on the tiles are depleted as the experiment proceeds, thus leading to a natural decrease of the Be II signal with time.

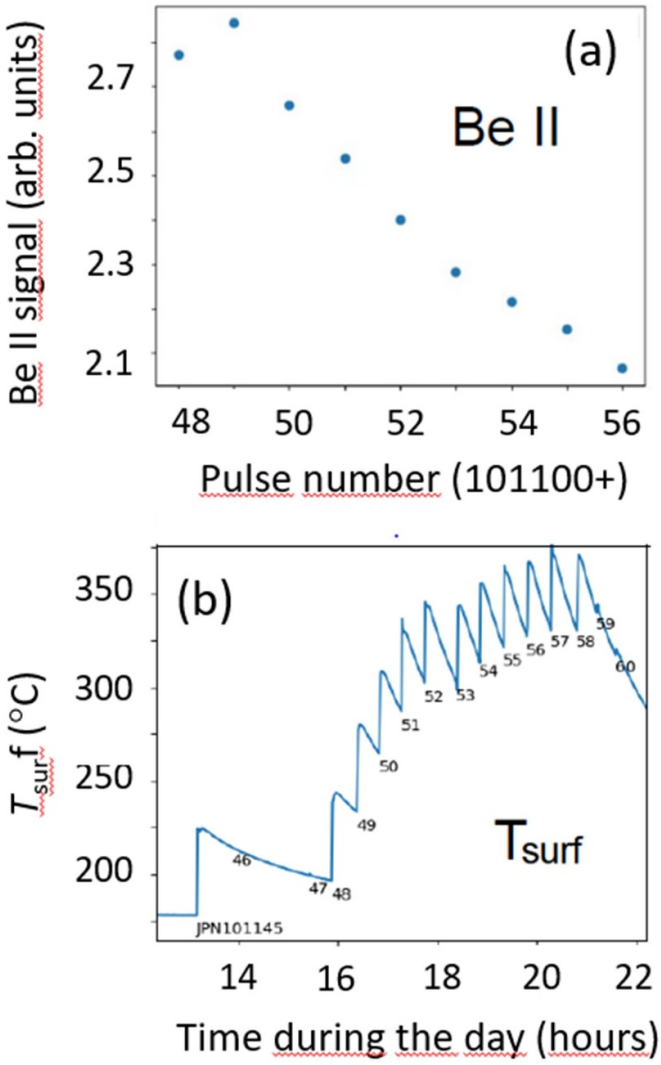

Figure 9. (*a*) Evolution of the Be II signal, indicative of erosion of Be limiter PFCs, as a function of the JET pulse number during the L-mode experiment. (*b*) Correspondence between the JET pulse number (numbers starting from 101 145 up to 101 160), the limiter temperature as well as the machine time (in hours) during the day of the experiment.

3.4.2. Production of W fuzz in helium. The formation of nanostructures on W surfaces upon exposure to helium plasmas was unambiguously demonstrated on AUG [10]. The experiment was based on a long flat-top scenario at $I_p = 0.8$ MA and $B_t = 2.5$ T and with the samples mounted on the DIM-II manipulator as shown in figure 1. In the H-mode phase, 8 discharges at a heating power of 6.2 MW of NBI and 4.3 MW of ECRH were executed while in the L-mode phase, 6 discharges were run with ECRH only (power ∼1 MW). In H-mode, the conditions were favourable for creating fuzz on the surface as the following shows:

- The He fluence reached the value of 3.4×10^{24} m^{-2} close to the strike point and decreased down to $\sim 2 \times 10^{24}$ m^{-2} on the peripheral samples towards higher values of the poloidal coordinate (the two topmost samples in figure 1) [10]. This is under the realistic assumption that the dominant species in the edge plasma is He^{2+}. In any case, the measured fluences are well above the threshold value of 10^{24} m^{-2} mentioned in section 2.1.1.
- The measured electron temperature around the strike point was >20 eV, corresponding to an energy of >100 eV for singly-ionized He^+ ions and >160 eV for the doubly-charged He^{2+} particles [7]. Thus, the requirement for 20 eV for the energy of the impinging particles was clearly exceeded.
- The surface temperature could not be measured accurately since the applied infrared camera saturated at the early stages of the plasma discharges. However, at least values of 1800 K could be reached in the strike point (extrapolated to climb up to 2500 K) [10]. Moreover, on all the samples positioned at the SOL side of the strike point the surface temperatures increased above the previously mentioned temperature limit of 1000 K during several seconds of each discharge.

In the L-mode part of the experiment, the fluence was an order of magnitude lower than in H-mode, the energy of

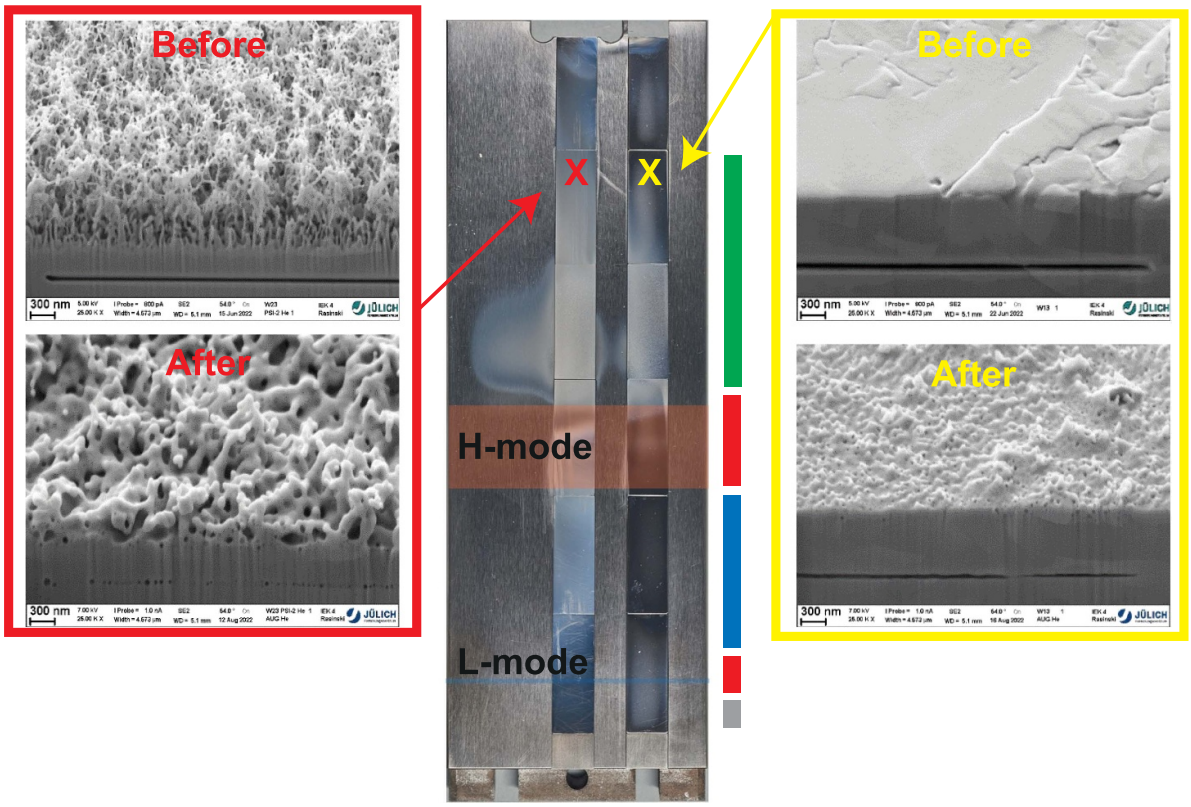

Figure 10. Photograph of the bulk W and nanostructured W samples mounted on the DIM-II manipulator head after the AUG plasma experiment together with SEM images from selected spots before and after the plasma exposure. Changes in the surface structure and morphology are clearly visible. The coloured bars on the right side of the photograph denote the characteristic poloidal regions on the samples: green = strong formation of nanostructures including W fuzz, red = dominated by erosion, blue = covered with deposits, and grey = no apparent changes. The L-mode and H-mode strike point regions are marked with light blue and red stripes in the figure, respectively.

the incoming particles was comparable to what had been measured in H-mode, while the surface temperature was clearly reduced. In this regime, the plasma conditions favoured erosion and deposition of the PFC material instead of nanostructure formation.

The AUG samples showed different characteristic regions along the tile surfaces in the poloidal direction as figure 10 summarizes. No visible surface modifications were present below the L-mode strike point (grey), whereas noticeable erosion had taken place around both the L-mode and H-mode strike lines (red). In between the two strike points, co-deposited layers covered the underlying surface features (blue); the co-deposited layers on the samples were up to 250 nm thick and consisted predominantly of W and O.

Clear fuzz formation was finally evidenced in a relatively broad poloidal region above the H-mode strike point (green). Besides fuzz creation, samples with pre-existing fuzz from PSI-2 exposure showed either removal or modifications of their surface nanofeatures. The results prove that W fuzz can grow in typical operational conditions of a tokamak, even with type-I ELMy H-mode plasmas but somewhat outside of the region with the most intense particle loads. Please note from figure 10 that fuzz has also formed on the DIM-II target tiles (made of W), as evidenced by the distinct bluish–whitish area to the left of the third (from the top) PSI-2 treated sample. It is worth pointing out that this region is not black which is the characteristic colour for W with nanostructures formed on it.

Overall, the picture agrees with the analysis of the samples exposed in the 2019 helium campaign, however, on those samples Mo was a dominant impurity and the roles of Mo and W in the formation of nanostructures on those samples could not be distinguished [43]. Compared to the 2015 experiment [7], the amount of boron remains at a low level, also in the private flux region of either the H- or L-mode experiment. This proves the crucial role of boronizations in determining the migration of light impurities in a tokamak: the 2015 experiment was carried out close to a boronization, the 2019 and 2022 ones far from it.

The formation of the fuzz in the present experiment was very non-uniform and reflected variations in the surface-temperature profile of the exposed samples and on the target tile. Thicknesses up to 1 μm could be measured for the created fuzz layer but the individual tendrils showed a large range of heights and widths; the thickest protrusions were formed closer to the strike point while poloidally further away, a fine-grained mesh became visible.

On JET, for its part, a scenario with reasonably long discharges (I_p = 1.7 MA, B_t = 2.0 T) in an ELMy H-mode was established. However, the ELM frequency was relatively large (~110 Hz) and obtained close to the LH threshold. Assuming

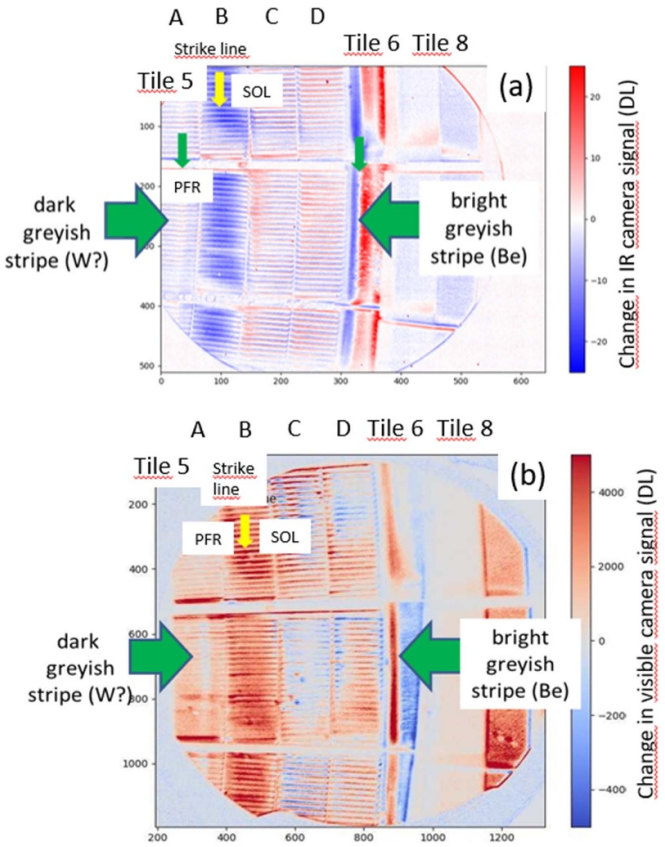

Figure 11. Differential images (subtraction of images taken before and after the W fuzz experiment) of the JET divertor recorded by (*a*) an IR camera and (*b*) a visible camera. The relevant divertor tiles (tiles 5, 6, and 8 as well as the four stacks of tile 5) are marked in the images together with the strike line, PFR, and SOL regions. The dark/bright greyish stripes identified after the experiment are also marked in the figure.

equal ratio for the He^{2+} and He^{+} ions, the incident ion energy was estimated to >100 eV (similarly to the case on AUG) and the total fluence $>10^{25}$ m^{-2} during the 54 discharges. The surface temperature close to the strike point was measured to >1200 K at this fluence, thus by all known criteria, the limit for fuzz creation was exceeded. The experiment is introduced and discussed in [44].

Despite the conditions being favourable for nanostructure formation, no obvious signs of fuzz creation could be observed, particularly no changes in the colours of the sample surface. After the experiment, visual inspection by infrared (IR) and visible cameras revealed a darkish stripe at the private flux region (PFR) and a wide greyish one almost at the edge of tile on the SOL side, next to the neighbouring tile 6 (see figure 11). Both of these could equally well be explained by co-deposition with W and Be but a full surface analysis can only be done once the tiles are removed from the vessel. We speculate that the growing fuzz is eroded by the large number of ELMs (>30 000 events in the type-III regime) impinging on the surface and further masked by the strong influx of Be from the main chamber. Similarly puzzling result has been obtained on WEST during its helium campaign: no signs of W fuzz even if the main criteria were considered to be met [45].

4. Discussion and conclusions

Experimental campaigns in helium plasmas were carried out on AUG and JET under the Tokamak Exploitation Task Force of the EUROfusion Consortium with the focus on addressing key research topics put forward in the ITER Research Plan. In particular, the following questions were high on the experimental agenda: (i) Is it feasible to carry out non-nuclear operations in ITER using helium plasmas with distinct type-I ELMy behaviour and (ii) how would the PWI mechanisms differ from the established picture in deuterium?

The experiments revealed that accessing the type-I ELMy regime is possible in helium but there are no apparent advantages over the other non-nuclear plasma species, hydrogen. Whilst the L-H transition power threshold can be lower, entering the type-I regime may require equally much (or potentially even more) heating power in He than in H. The pedestal characteristics and confinement properties in He plasmas appear to be comparable to those determined for hydrogenic plasmas, however, more peaked density profiles in He indicate changes in the particle transport. More analysis is also needed to fully understand the power transport, since based on earlier data confinement had been observed to be reduced in He compared to the case in D.

On the side of the edge plasma, particle recycling at the divertor was smaller in He than in D and higher densities were needed for the onset of detachment, potentially because of the lack of molecular channels to assist detachment in He plasmas. On the other hand, reaching the desired purity of He plasmas is relatively straightforward whereas subsequent operations in H or D require special cleaning efforts and engineering solutions to ensure efficient pumping of the released compounds. Considering fuel retention, helium pulses led to a higher retention of He than removal of hydrogen isotopes but, on the other hand, the overall retention was not particularly strong unlike what can be the outcome in H or D. The post-exposure analyses of the fuel inventory, especially that of He, are still pending and will be reported elsewhere.

In the field of plasma-surface interactions, physical sputtering and net erosion of W were quite expectedly increased in He compared to H or D plasmas, mainly due to the higher mass and the contribution from the He^{2+} ions. Surface nanostructures (W fuzz) were demonstrated to form under tokamak conditions, albeit there is a delicate balance between erosion, deposition, surface annealing, and nanostructure formation locally on the PFCs [44]. This is sensitively dependent on the applied plasma scenario as well as on the distance from the strike point at the divertor as the experiments on AUG and JET have demonstrated. On the other hand, the absence of direct proof for W fuzz creation after tens of thousands of ELMs on JET divertor tiles can also indicate that in ITER helium would not cause insurmountable problems for the PFC lifetime.

As a conclusion, helium plasmas remain possible candidates to be used in the non-nuclear phases of ITER, however, no clear conclusion can be drawn on the added value of He over that of H. On the other hand, helium will become an

important factor in the nuclear phase of ITER, thus our studies have helped in deepening the understanding of He particle behaviour in fusion plasmas and their impact on the lifetime of the reactor wall and retention of fuel on it. The results of these experiments have already had consequences for the ITER plans. In fact in the new baseline Research Plan [3], ITER is considering demonstrating H-mode scenarios in D and not anymore in H or He under conditions specifically optimized for low neutron production.

Acknowledgments

This work has been carried out within the framework of the EUROfusion Consortium, partially funded by the European Union via the Euratom Research and Training Programme (Grant Agreement No 101052200—EUROfusion). The Swiss contribution to this work has been funded by the Swiss State Secretariat for Education, Research and Innovation (SERI). Views and opinions expressed are however those of the author(s) only and do not necessarily reflect those of the European Union, the European Commission or SERI. Neither the European Union nor the European Commission nor SERI can be held responsible for them. The views and opinions expressed herein do not necessarily reflect those of the ITER Organization. This research was supported in part by the grants FIS2017-85252-R and PID2021-127727OB-I00, funded by MCIN/AEI/ 10.13039/501100011033 and by 'ERDF A way of making Europe'.

ORCID iDs

M. Balden https://orcid.org/0000-0002-8755-9370
R. Bisson https://orcid.org/0000-0002-8819-1563
S. Brezinsek https://orcid.org/0000-0002-7213-3326
T. Dittmar https://orcid.org/0000-0002-4325-7979
L. Garzotti https://orcid.org/0000-0002-3796-9814
M. Groth https://orcid.org/0000-0001-7397-1586
A. Kappatou https://orcid.org/0000-0003-3341-1909
K. Krieger https://orcid.org/0000-0003-0427-8184
B. Labit https://orcid.org/0000-0002-0751-8182
A. Loarte https://orcid.org/0000-0001-9592-1117
M. Maslov https://orcid.org/0000-0001-8392-4644
D. Matveev https://orcid.org/0000-0001-6129-8427
R.A. Pitts https://orcid.org/0000-0001-9455-2698
U. Plank https://orcid.org/0000-0002-1509-4308
M. Rasinski https://orcid.org/0000-0001-6277-4421
D. Ryan https://orcid.org/0000-0002-7735-3598
S. Saarelma https://orcid.org/0000-0002-6838-2194
S. Silburn https://orcid.org/0000-0002-3111-5113
E.R. Solano https://orcid.org/0000-0002-4815-3407
W. Suttrop https://orcid.org/0000-0003-0983-8881
T. Tala https://orcid.org/0000-0002-6264-0797
N. Vianello https://orcid.org/0000-0003-4401-5346
T. Wauters https://orcid.org/0000-0002-2941-7817
A. Widdowson https://orcid.org/0000-0002-6805-8853

References

[1] Kikuchi M. and Azumi M. 2015 Tokamak Fusion Reactor *Frontiers in Fusion Research II–Introduction to Modern Tokamak Physics* (Springer)
[2] ITER ORGANIZATION 2018 *ITER Research Plan within the Staged Approach ITR-18-003* (available at: www.iter.org/doc/www/content/com/Lists/ITER%20Technical%20Reports/Attachments/9/ITER-Research-Plan_final_ITR_FINAL-Cover_High-Res.pdf)
[3] Barabaschi P. *et al* 2023 The ITER project—progress on manufacturing, construction, commissioning and an updated baseline *Preprint: 2023 IAEA Fusion Energy Conf. (London, UK, 16–21 October 2023)* [OV/1-3]
[4] Stroth U. *et al* 2022 *Nucl. Fusion* **62** 042006
[5] Mailloux J. *et al* 2022 *Nucl. Fusion* **62** 042026
[6] Loarte A. *et al* 2021 *Nucl. Fusion* **61** 076012
[7] Hakola A. *et al* 2017 *Nucl. Fusion* **57** 066015
[8] Zastrow K.-D. *et al* 2005 *Nucl. Fusion* **45** 163
[9] Herrmann A. *et al* 2015 *Fusion Eng. Des.* **98–99** 1496
[10] Rasínski M. *et al* 2023 *Nucl. Mater. Energy* **37** 101539
[11] Petty T.J., Baldwin M.J., Hasan M.I., Doerner R.P. and Bradley J.W. 2015 *Nucl. Fusion* **55** 093033
[12] Wright J.A.R. 2022 *Tungsten* **4** 184
[13] Hakola A. *et al* 2021 *Nucl. Fusion* **61** 116006
[14] Pearce R.J., Antipenkov A., Boussier B., Bryan S., Dremel M., Levesy B., Mayaux C. and Wykes M. 2013 *Fusion Eng. Des.* **88** 809–13
[15] Wauters T. *et al* 2024 *Nucl. Mater. Energy* **38** 101587
[16] Matveev D. *et al* 2023 *Nucl. Fusion* **63** 112014
[17] Kovtun Y. *et al* 2023 *Nucl. Mater. Energy* **37** 101521
[18] Bisson R. *et al* 2021 *Nucl. Mater. Energy* **26** 100885
[19] Plank U. *et al* 2023 *Plasma Phys. Control. Fusion* **65** 014001
[20] Solano E.R. *et al* 2021 *Nucl. Fusion* **61** 124001
[21] Solano E.R. *et al* 2022 *Nucl. Fusion* **62** 076026
[22] Huber A. *et al* 2021 *Phys. Scr.* **96** 124046
[23] Maslov M. *et al* 2023 ELMy H-mode Helium plasma at JET-ILW *49th European Physical Society Conf. on Plasma Physics (Proc. Int. Conf.) (Bordeaux, France, 3–7 July 2023)*
[24] McDonald D.C. *et al* 2004 *Plasma Phys. Control. Fusion* **46** 519
[25] McDonald D.C. *et al* 2010 JET Helium-4 ELMy H-mode studies *23rd IAEA Fusion Energy Conf. EXC/2-4Rb (Proc. Int. Conf.) (Daejon, Republic of Korea, 11–16 October 2010)*
[26] Martin Y.R. *et al* 2008 *J. Phys.: Conf. Ser.* **123** 012033
[27] Saarelma S., Challis C.D., Garzotti L., Frassinetti L., Maggi C.F., Romanelli M. and Stokes C. 2018 *Plasma Phys. Control. Fusion* **60** 014042
[28] Suttrop W. *et al* 2018 *Nucl. Fusion* **58** 096031
[29] Suttrop W. *et al* 2023 Loss of ELM suppression with non-axisymmetric magnetic perturbations in ASDEX Upgrade helium plasmas *49th European Physical Society Conf. on Plasma Physics (Proc. Int. Conf.) (Bordeaux, France, 3–7 July 2023)*
[30] Willensdorfer M. *et al* 2023 Resistive and 3D effect in ELM-suppressed H-mode and the L-H power threshold with resonant magnetic perturbations in ASDEX Upgrade *Preprint: 2023 IAEA Fusion Energy Conf. (London, UK, 16–21 October 2023)* [EX/6-1R]
[31] Leuthold N. *et al* 2024 *Nucl. Fusion* **64** 026017
[32] Kiefer C.K., Angioni C., Tardini G., Bonanomi N., Geiger B., Mantica P., Pütterich T., Fable E. and Schneider P.A. 2021 *Nucl. Fusion* **61** 066035
[33] Angioni C., Gamot T., Tardini G., Fable E., Luda T., Bonanomi N., Kiefer C.K. and Staebler G.M. (the ASDEX Upgrade Team and the EUROfusion MST1 Team) 2022 *Nucl. Fusion* **62** 066015

[34] Manas P., Angioni C., Kappatou A., Ryter F. and Schneider P.A. 2019 *Nucl. Fusion* **59** 014002
[35] Tala T. *et al* 2023 *Nucl. Fusion* **63** 112012
[36] Rees D. *et al* 2023 Characterisation of the scrape-off layer in JET-ILW deuterium and helium low-confinement mode plasmas *19th Int. Conf. on Plasma-Facing Materials and Components for Fusion Applications (Proc. Int. Conf.)* (*Bonn, Germany*, *22–26 May 2023*)
[37] Karhunen J., Holm A., Aleiferis S., Carvalho P., Groth M., Lawson K.D., Lomanowski B., Meigs A.G., Shaw A. and Solokha V. 2023 *Nucl. Mater. Energy* **34** 101314
[38] Brezinsek S., Stamp M.F., Nishijima D., Borodin D., Devaux S., Krieger K., Marsen S., O'Mullane M., Bjoerkas C. and Kirschner A. 2014 *Nucl. Fusion* **54** 103001
[39] Doerner R.P., Baldwin M.J., Buchenauer D., De Temmerman G. and Nishijima D. 2009 *J. Nucl. Mater.* **390–391** 681
[40] Baldwin M. and Doerner R.P. 2008 *Nucl. Fusion* **48** 035001
[41] Tokunaga K., Doerner R.P., Seraydarian R., Noda N., Kubota Y., Yoshida N., Sogabe T., Kato T. and Schedler B. 2003 *J. Nucl. Mater.* **313–316** 92
[42] Vuoriheimo T. *et al* 2024 Erosion on divertor during helium plasma operation in ASDEX Upgrade *26th Int. Conf. on Plasma Surface Interaction in Controlled Fusion Devices (Proc. Int. Conf.)* (*Marseille, France, 12–17 May 2024*)
[43] Balden M. *et al* 2024 Microscopy study of the growth and erosion of fuzz on tungsten by helium plasma exposure on ASDEX Upgrade *24th Int. Conf. on Plasma Surface Interactions in Controlled Fusion Devices* (*Virtual*, *25–29 January 2021*)
[44] Brezinsek S. *et al* 2023 The competition between W nanostructure formation and W annealing, W erosion and low-Z co-deposition in the divertor of metallic fusion devices *Preprint: 2023 IAEA Fusion Energy Conf.* (*London, UK*, *16–21 October 2023*) [EX/P7-27]
[45] Tsitrone E. *et al* 2022 *Nucl. Fusion* **62** 076028